

applied optics

Effect of the measuring mirror surface shape error on ruled groove straightness and the grating diffraction wavefront

XIAOTAO MI,* D SHANWEN ZHANG, XIANGDONG QI, HAILI YU, HONGZHU YU, SIBO JIANG, YU LIN, JINGXUAN ZHOU, AND YEYAO SUN

Changchun Institute of Optics, Fine Mechanics and Physics, Chinese Academy of Sciences, Changchun Jilin 130033, China *Corresponding author: mixiaotao_ciomp@126.com

Received 2 June 2020; revised 24 August 2020; accepted 24 August 2020; posted 25 August 2020 (Doc. ID 399147); published 18 September 2020

Measuring mirror requirements and their impact on groove errors are related to the error compensation strategy for a ruling engine. We analyze why the measuring mirror of the CIOMP-6 engine affects the groove straightness and the grating diffraction wavefront. We study a theoretical model of the relationship between the measuring mirror's surface shape error and the grating wavefront, propose a requirement for the measuring mirror surface shape error, and reprocess the measuring mirror. Comparative ruling experiments prove that the grating's wavefront quality at the diffraction order along the groove direction improved significantly after reprocessing of the measuring mirror. © 2020 Optical Society of America

https://doi.org/10.1364/AO.399147

1. INTRODUCTION

The excellence of grating functions such as their dispersion, polarization, and phase matching have led to strong demand for these elements in application areas such as spectral analysis [1,2], lasers [3,4], optical communications [5,6], and pulse compressors [7,8]. The mechanical ruling method, which is one of the most important grating production methods, is mainly used to produce gratings with high-quality, high-precision, and strictly controlled shapes such as echelle gratings and infrared laser gratings [9,10].

The grating ruling engine is a mother machine used to fabricate the ruled grating masters [11–13]. The accuracy of the grating ruling engine affects the ruled grating accuracy directly. All of the grating groove position errors, with the exception of the grating blank surface shape error caused by substrate processing and the grating substrate coating [14], are caused by the grating ruling engine [15,16]. The grating groove straightness is an important factor that affects both the grating wavefront error and the grating resolution. In the case where the index requirements of the grating remain the same, when the grating size becomes larger and the ruled groove length increases, the ruled groove straightness requirement will also increase.

Almost all ruling engines guarantee the straightness of their grating grooves through the precision of the diamond carriage guide used [11,12,17,18]. The most representative grating ruling engine is the internationally known MIT-C engine in

the USA, which is currently the world's largest ruling engine and has the ability to rule blanks with dimensions of up to $450 \text{ mm} \times 650 \text{ mm} \times 125 \text{ mm}$. In the MIT-C engine, the diamond carriage guides include both a cylindrical metal rail and a square fused-silica rail. The cylindrical metal rail, which consists of Nitralloy cylinders that are 62.5 mm in diameter and 1000 mm long, is straight to within a fringe and is mainly used to carry the weight of the diamond carriage; the square fusedsilica rail, with dimensions of $100 \text{ mm} \times 100 \text{ mm} \times 510 \text{ mm}$, is straight to within one-fourth of a fringe with no abrupt departures and is mainly used for guidance of the diamond carriage. The diamond carriage hangs from slide bearings that ride on an overhead cylindrical rail and is restricted to straight-line motion using a Rulon-covered button that presses against a fused-silica straight edge. Therefore, the flatness of the contact surface between the fused-silica rail and the button located on the diamond carriage determines the grating groove straightness [18].

Unlike other grating ruling engines, the straightness of the grating groove in the CIOMP-6 ruling engine is mainly affected by the measuring mirror's surface shape error [19]. In this paper, we analyze the reasons why the measuring mirror affects the groove straightness and the grating diffraction wavefront. We then establish a mathematical model of the relationship between the measuring mirror's surface shape error and the grating wavefront. Finally, we reprocess the measuring mirror, which greatly

improves the wavefront quality for the grating along the groove direction.

2. EFFECT OF THE MEASURING MIRROR SURFACE SHAPE ON GROOVE STRAIGHTNESS IN THE CIOMP-6 ENGINE

In previous works [13,19], we have provided a detailed introduction to the CIOMP-6 ruling engine, including its blank carriage system, its new diamond carriage system that uses aerostatic guideways, the new high-precision engine control strategies, the groove error measurement system, the closed-loop engine control system, and its ruling ability and the accuracy of the gratings. In this paper, we therefore only provide a summary description of the parts of the ruling engine related to the work in the paper.

The CIOMP-6 ruling engine uses a stop-and-go blank motion action, and the blank carriage system remains stationary during grating ruling. Similar to other closed-loop-controlled ruling engines, the early closed-loop control method used for the CIOMP-6 engine realized groove positioning by adjusting the carriage with a blank, and the grating groove's straightness was guaranteed by the diamond carriage guide. As shown in Fig. 1, the CIOMP-6 ruling engine uses aerostatic guideways for the diamond carriage. The straightness of the slider that runs along the guide over a range of 500 mm is better than 0.05 in., while the groove error caused by deflection of the slider relative to the guide is less than 10 nm. The accuracy of this guide thus meets the requirements for the ruling of high-precision gratings. Under dark conditions, a laser beam that needs to be measured incidents on the ruled grating surface at a designed angle of incidence, and then we use a moving power meter to measure the power, including the blazed order and the ghosts or scattered light between the diffraction orders; the ratio of the maximum power of the ghosts or scattered light to the blazed-order power is defined as the ghosts or scattered light intensity; the strongest intensity of the light scattered from the ruled grating cannot reach the level of 10^{-4} , which is related to the blank carriage correction system used for the groove position errors correction. The ability of our blank carriage to correct the groove errors and the mechanical natural frequency of the blank carriage contradict each other; for large-area gratings, the mass of the inner carriage plus that of the large-area grating blank may be as much as several hundred kilograms, and it is quite difficult to drive such heavy loads and simultaneously achieve nanometerscale control accuracy. Therefore, we propose a new idea for adjustment of the position error of the groove; in this approach, nanometer-scale groove positioning is achieved by adjusting the position of the lightweight diamond holder.

Using this new idea for the adjustment of the groove position error, we improved the CIOMP-6 engine, as shown in Fig. 2. We designed a new and complex diamond carriage that had a laser interferometer and a piezoelectric drive device installed on it, while the diamond holder and the reference mirror were mounted on the moving carriage of the piezoelectric drive device. A mirror with dimensions of $100 \, \mathrm{mm} \times 80 \, \mathrm{mm} \times 420 \, \mathrm{mm}$ that was mounted on the blank carriage is used as a measuring mirror. During ruling engine

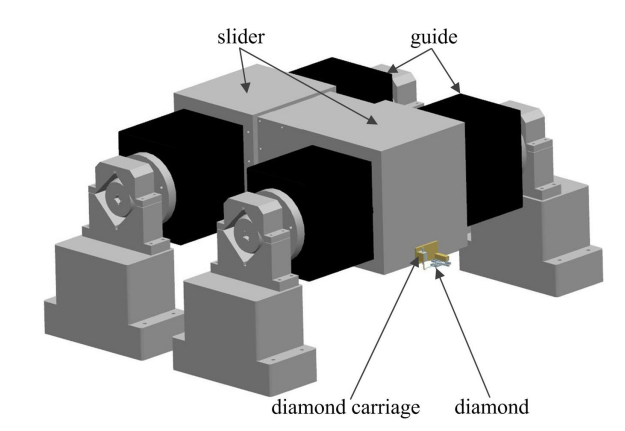


Fig. 1. Schematic diagram of the guideways used for the diamond carriage.

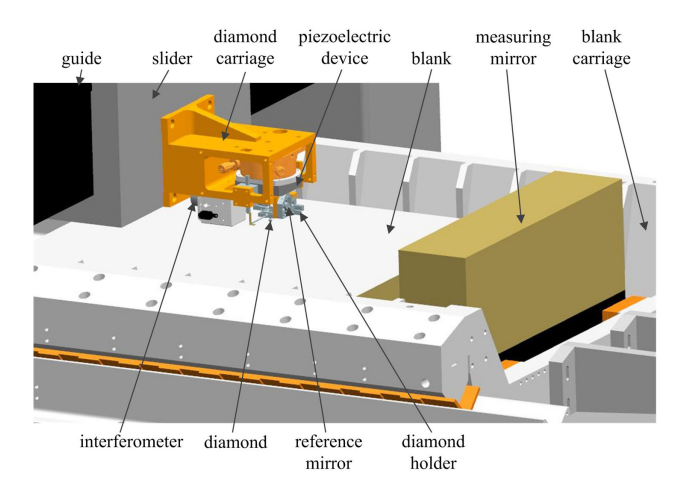


Fig. 2. Schematic diagram of the improved mechanical structure.

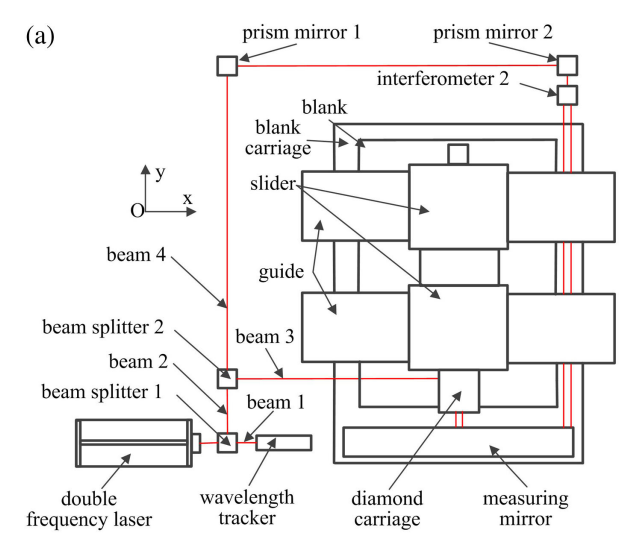
operation, we believe that the reference mirror and the measuring mirror remain relatively stationary with reference to the diamond and the blank, respectively.

The grating grooves to be ruled are a set of parallel straight lines at equal intervals. Before a grating is ruled, the yaw error and the accumulated error generated during operation of the blank carriage have been corrected, and then the blank carriage has come to a standstill after running over a range of hundreds of nanometers from the theoretical ruling position. When the grating is ruled, the piezoelectric device drives the diamond in real time to adjust the groove error; the amount of this adjustment is determined using the value obtained from the theoretical position of the grating groove, the value measured using the interferometer, and the Abbe error correction relationship. Therefore, if we compare the blank and the diamond to a blank paper and a pen, respectively, the measuring mirror acts like a standard ruler; ruling a grating groove is like drawing a straight line on a blank paper with a pen along the ruler. The flatness of the measuring mirror will affect the straightness of the grating grooves directly, so we require the flatness of the measuring mirror to be as high as possible.

3. MATHEMATICAL MODEL OF THE MEASURING MIRROR SURFACE SHAPE ERROR AND THE GRATING DIFFRACTION WAVEFRONT

Based on the proposed idea and the improved structure, the new measurement optical path structure for the CIOMP-6 engine is shown in Fig. 3. A laser beam with $\lambda=632.8$ nm from a double-frequency laser is split into two beams using beam splitter 1. Beam 1 is then incident into a wavelength tracker to compensate for the groove errors caused by changes in the refractive index of the air. Beam 2 is split further into two beams using beam splitter 2. Beam 3 is incident into interferometer 1 on the diamond carriage and is used to measure the displacement error between the reference mirror and the measuring mirror. Beam 4 is incident into interferometer 2 via prism mirror 1 and prism mirror 2 and is subsequently used to measure the blank carriage pitch error.

The reason for the design of optical beam 4 is that the rule of the Abbe principle is not followed when measuring the groove error, i.e., an Abbe error will be generated because the ruling plane and the measurement plane do not coincide. The Abbe error is mainly caused by the pitch during operation of the blank carriage. As shown in Fig. 4, the distance between the two measuring beams of interferometer 2 is l_1 , and the distance between the measurement plane and the ruling plane is l_2 ; at any groove i, the groove error measured by interferometer 1 is η_{i3} , the groove errors of the upper and lower optical paths measured by interferometer 2 are η_{i1} and η_{i2} , respectively, and then the Abbe error angle α_i and the groove error η_{i4} that must be corrected for the ruling plane are as shown in Eq. (1):



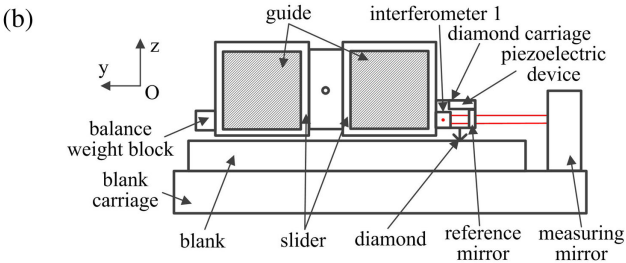


Fig. 3. Optical path structure of the CIOMP-6 engine. (a) Top view; (b) side view.

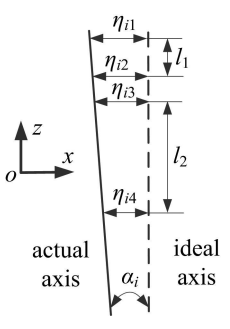


Fig. 4. Schematic diagram of the Abbe error.

$$\begin{cases} \alpha_i = \arctan\left(\frac{\eta_{i1} - \eta_{i2}}{l_1}\right) \\ \eta_{i4} = \eta_{i3} - l_2 \cdot \tan \alpha_i = \eta_{i3} - l_2 \cdot \frac{\eta_{i1} - \eta_{i2}}{l_1} \end{cases} . \tag{1}$$

It is precisely the long narrow area of the measuring mirror that is used for the laser beam that affects the position errors of the grooves. The blank carriage pitch angle is so small that the groove position error at the same position on different grooves is identical. We sampled every groove at equal intervals, and the number of samples taken was m. The cross-sectional profile of the long narrow area of the measuring mirror that is used for grating ruling can be expressed as

$$\delta_0 = \begin{bmatrix} \delta_1 \\ \delta_2 \\ \vdots \\ \delta_m \end{bmatrix}. \tag{2}$$

Combining Eqs. (1) and (2) allows the effect of the error δ_0 on the position error of groove i to be given as

$$\delta_{i} = \delta_{0} - l_{2} \cdot \tan \alpha_{i} = \begin{bmatrix} \delta_{1} \\ \delta_{2} \\ \vdots \\ \delta_{m} \end{bmatrix} - l_{2} \cdot \frac{\eta_{i1} - \eta_{i2}}{l_{1}}$$

$$= \begin{bmatrix} \delta_{1} - l_{2} \cdot \frac{\eta_{i1} - \eta_{i2}}{l_{1}} \\ \delta_{2} - l_{2} \cdot \frac{\eta_{i1} - \eta_{i2}}{l_{1}} \\ \vdots \\ \delta_{m} - l_{2} \cdot \frac{\eta_{i1} - \eta_{i2}}{l_{1}} \end{bmatrix}.$$
(3)

The blank carriage remains stationary during grating ruling, so the Abbe error angle α_i is a fixed value for different positions of the same groove, and the groove profile is similar to the cross-sectional profile of the long narrow area of the measuring mirror.

The yaw error and the accumulated error have been compensated before the grating is ruled, and their residual error is a random error that mainly affects the scattered light and does not affect the grating wavefront. Regardless of the effects of the yaw error and the accumulated error on the grooves, if we suppose that the number of grating grooves is n, then the position error of the grooves for the entire grating can be given as

$$\delta_{nm} = [\delta_{1} \cdots \delta_{i} \cdots \delta_{n}] = \begin{bmatrix} \left(\delta_{1} - l_{2} \cdot \frac{\eta_{11} - \eta_{12}}{l_{1}}\right) & \cdots \left(\delta_{1} - l_{2} \cdot \frac{\eta_{i1} - \eta_{i2}}{l_{1}}\right) \cdots \left(\delta_{1} - l_{2} \cdot \frac{\eta_{n1} - \eta_{n2}}{l_{1}}\right) \\ \left(\delta_{2} - l_{2} \cdot \frac{\eta_{11} - \eta_{12}}{l_{1}}\right) & \cdots \left(\delta_{2} - l_{2} \cdot \frac{\eta_{i1} - \eta_{i2}}{l_{1}}\right) \cdots \left(\delta_{2} - l_{2} \cdot \frac{\eta_{n1} - \eta_{n2}}{l_{1}}\right) \\ \vdots \\ \left(\delta_{m} - l_{2} \cdot \frac{\eta_{11} - \eta_{12}}{l_{1}}\right) & \cdots \left(\delta_{m} - l_{2} \cdot \frac{\eta_{i1} - \eta_{i2}}{l_{1}}\right) \cdots \left(\delta_{m} - l_{2} \cdot \frac{\eta_{n1} - \eta_{n2}}{l_{1}}\right) \end{bmatrix}.$$

$$(4)$$

As shown in Eq. (4), the abscissa represents the same position along the ruling direction on different grooves, and the coordinates represent the different grooves.

However, when the grating is ruled, we compensate for the groove error caused by the Abbe error and believe that the error δ_0 generated by the measuring reference mirror is equal to zero; in fact, the error δ_0 cannot be zero, so the groove error for the entire grating after ruling can be written as

$$\delta'_{nm} = \begin{bmatrix} \delta_1 & \delta_1 \cdots \delta_1 \\ \delta_2 & \delta_2 \cdots \delta_2 \\ \vdots \\ \delta_m & \delta_m \cdots \delta_m \end{bmatrix}.$$
 (5)

The effect of the measuring mirror surface shape error on the grating performance is described as follows: (1) the error of deflection toward the high frequency mainly affects the stray light and the ghost lines of the grating; and (2) the error of deflection toward the low frequency mainly affects the grating wavefront. The amplitude of the high-frequency error on the measuring surface is quite small, and the measured value is the result of homogenization of an area with a diameter of 3 mm, so the effect of the high-frequency error on the grating performance is so small that it can be ignored. The low-frequency error will affect both the diffraction wavefront and the resolution of the grating.

The grating diffraction equation is given as follows:

$$d \cdot (\sin \alpha + \sin \beta_m) = m \cdot \lambda, \tag{6}$$

where d is the grating constant, α is the angle of incidence, β_m is the mth-order diffraction angle, m is the grating diffraction order, and λ is the incident light wavelength.

The optical path difference caused by the groove error can be written as

$$\varepsilon = \delta'_{nm} \cdot (\sin \alpha + \sin \beta_m). \tag{7}$$

According to the principle of Zygo interferometer-based measurement, the essence of the wavefront error is the optical path difference. By combining Eqs. (5)–(7), the diffraction wavefront of the grating can be written as

$$\Delta(m) = \frac{m\lambda}{d} \cdot \delta'_{nm} = \frac{m\lambda}{d} \begin{bmatrix} \delta_1 & \delta_1 & \cdots & \delta_1 \\ \delta_2 & \delta_2 & \cdots & \delta_2 \\ \vdots & \vdots & \vdots \\ \delta_m & \delta_m & \cdots & \delta_m \end{bmatrix} .$$
 (8)

Equation (8) shows that the cross-sectional profile of any grating groove along the ruling direction is the same as the cross-sectional profile of the long narrow area of the measuring mirror used for the measuring beam. Therefore, we hope that the measuring mirror's surface shape error will be as small as possible.

4. RULING EXPERIMENT

A. Before Reprocessing of the Measuring Mirror

The diamond carriage system, the groove error compensation method, and the optical path structure of the CIOMP-6 ruling engine have been improved three times, and the use of the measuring mirror with its dimensions of $100 \text{ mm} \times 80 \text{ mm} \times 420 \text{ mm}$ has also changed. Before the groove error correction scheme was improved, the optical measurement path only used areas of the measuring mirror with a diameter of 25 mm located at both ends in the 420 mm direction, so the overall shape of the measurement mirror was not required. After the groove error correction scheme was improved, during fabrication of a 300 mm × 500 mm × 100 mm large-area echelle grating for a spectrometer mounted on the fiber arrayed solar optical telescope (FASOT) designed by the Yunnan Observatory of the Chinese Academy of Sciences, we discovered the problem of groove bending from the results of measurements of the grating wavefront, and analysis showed that the cause of the problem was the measuring mirror's surface shape error.

As shown in Fig. 5, before the surface shape quality of the measuring mirror is improved, the peak-to-valley (PV) value of the wavefront error for the entire surface of the measuring mirror is 0.79λ (hereinafter, $\lambda = 632.8$ nm), and the PV value for the surface profile of the area for the measuring beam is 0.223λ .

When the measuring mirror has the wavefront error profile shown in Fig. 5, the wavefront of the 300 mm \times 500 mm \times 100 mm large-area echelle grating at the diffraction order (-35th) ruled using the CIOMP-6 engine is as shown in Fig. 6. The PV value of the grating wavefront profile at the diffraction order along the groove direction is 0.506λ . If the groove error is only affected by the surface shape error of the measuring mirror, then the PV value of the wavefront error for the entire grating at the diffraction order will be 0.506λ , but the measured PV value of the wavefront error for the entire grating at the diffraction order is 1.441\(\lambda\). The reasons for the difference described above are as follows: the Abbe errors caused by the measurements and the changes in the refractive index of the air, which affect the groove position errors, are being investigated and improved and have not yet been controlled and compensated; in addition, the improved thickness nonuniformity of the large-area grating metal film still affects the grating diffraction wavefront [14].

A comparison of Fig. 5 with Fig. 6 shows that the surface/wavefront profile curves of the area of the measuring mirror used for the measuring beam and the grating at the diffraction order along the groove direction are similar; this indicates that the grating wavefront profile along the groove direction is mainly affected by the measuring mirror's surface shape error.

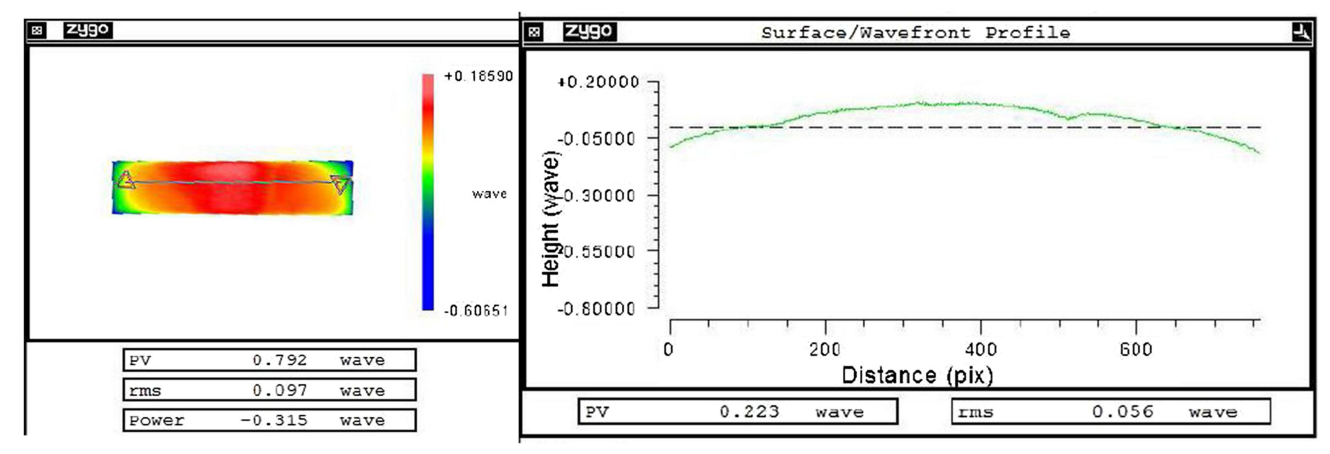


Fig. 5. Surface shape error of the measuring mirror before reprocessing, as measured using a Zygo interferometer.

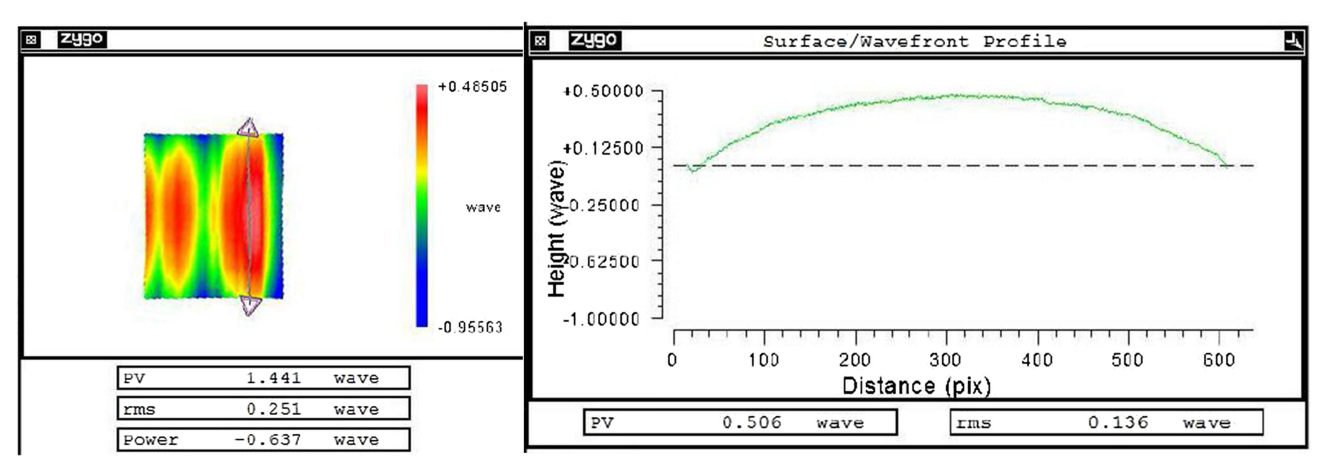


Fig. 6. Wavefront error of the grating diffraction order measured using the Zygo interferometer before reprocessing of the measuring mirror.

From the PV value of the surface profile of the area used for the measuring beam in Fig. 5, the PV value of the grating wavefront profile at the diffraction order along the groove direction is calculated using Eq. (8) to be 0.3902λ . The calculated PV value of 0.3902λ of the grating wavefront profile at the diffraction order along the groove direction is less than the measured PV value of 0.506λ . The reason for this difference between the theoretically calculated value and the actual measured value is that the improved thickness nonuniformity of the large-area grating metal film still affects the grating diffraction wavefront [14].

B. After Reprocessing of the Measuring Mirror

The CIOMP-6 engine is designed to rule blanks with dimensions of up to $400~\text{mm}\times500~\text{mm}\times100~\text{mm}$. If the wavefront of an echelle grating with dimensions of $400~\text{mm}\times500~\text{mm}\times100~\text{mm}$, a blazed order of -36, and a groove density of 79 grooves/mm is expected to be $\lambda/5$, then the PV value of the surface error of the area of the measuring mirror used for the laser beam is calculated using Eq. (8) to be $0.07032~\mu\text{m}$. When the existing optical processing capability and costs are considered, we require the surface shape error of the measuring mirror to be better than $\lambda/10$.

The surface shape error results for the measuring mirror after reprocessing are shown in Fig. 7, where the PV value of the wavefront error for the entire surface of the measuring mirror is 0.093λ , and the PV value of the surface profile of the area used for the measuring beam is 0.033λ .

After the improvement of the CIOMP-6 engine was completed, we used the measuring mirror, for which the wavefront error is shown in Fig. 7, as the measurement reference, and the wavefront of the 300 mm \times 500 mm \times 100 mm large-area echelle grating at the diffraction order (-35th) is shown in Fig. 8. The PV value of the wavefront error for the entire grating at the diffraction order is 0.297 λ , and the PV value of the grating wavefront profile at the diffraction order along the groove direction is 0.134 λ . The main reason for the difference between the PV value of the wavefront error for the entire grating and the PV value of the grating wavefront profile along the groove direction is the improved thickness nonuniformity of the large-area grating metal film and the residual error after compensation for the changes in the refractive index of the air.

A comparison of Fig. 7 with Fig. 8 shows that the surface/wavefront profile curves of the area of the measuring mirror used for the measuring beam and the grating at the diffraction order along the groove direction are not similar, and the surface shape error of the measuring mirror is thus no longer

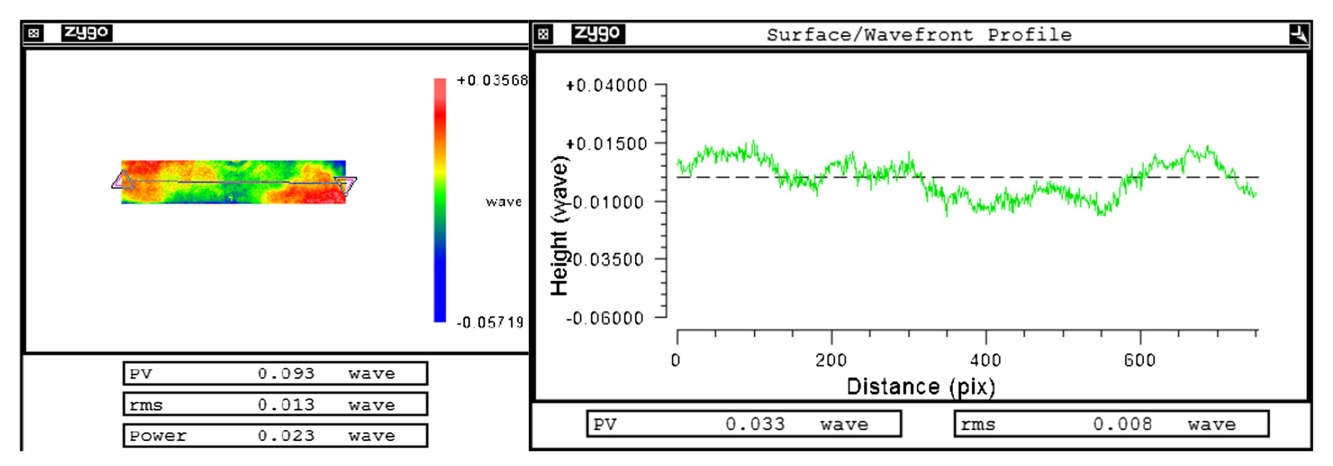


Fig. 7. Surface shape error of the measuring mirror after reprocessing, as measured using the Zygo interferometer.

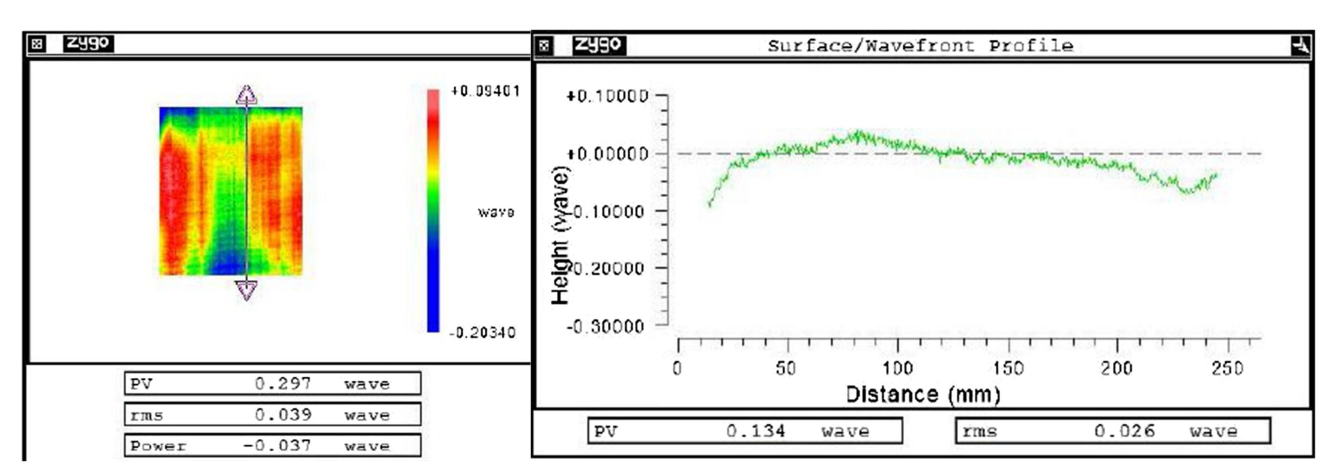


Fig. 8. Wavefront error of the grating diffraction order measured using the Zygo interferometer after reprocessing of the measuring mirror.

the main factor affecting the grating wavefront. From the PV value of the surface profile of the area used for the measuring beam in Fig. 7, the PV value of the grating wavefront profile at the diffraction order along the groove direction is calculated using Eq. (8) to be 0.0577λ , which is less than the measured PV value of 0.134λ shown in Fig. 8. As before, the surface shape quality of the measuring mirror is improved, and the main factor in the difference between the theoretically calculated value and the actual measured value is the effect of the thickness nonuniformity of the large-area grating metal film [14].

5. CONCLUSIONS

We introduced the effect of the measuring mirror surface shape error on the ruled groove straightness and the grating diffraction wavefront based on a new correction method for the groove position error adopted in the CIOMP-6 ruling engine. We then established a mathematical model of the relationship between the measuring mirror's surface shape error and the grating wavefront and proposed that the surface shape error of the measuring mirror with its dimensions of $100 \text{ mm} \times 80 \text{ mm} \times 420 \text{ mm}$ needed to meet the requirement of $\lambda/10$. After the measuring mirror was reprocessed, the surface shape error of the measuring mirror decreased from 0.79λ to 0.093λ . We ruled an echelle

grating before and after the improvement in the measuring mirror shape error. The ruling experiments proved that the grating wavefront quality at the diffraction order along the groove direction improved significantly in tandem with the improvements in the surface shape error of the measuring mirror.

Funding. Ministry of Science and Technology of the People's Republic of China (2016YFF0102006, 2016YFF0103304).

Acknowledgment. We are very grateful to Prof. Zhongquan Qu and his team for their trust and for selecting us to fabricate the grating that their work required; it is their demand for large-scale gratings that promotes further improvements in the accuracy of the CIOMP-6 ruling engine.

Disclosures. The authors declare no conflicts of interest.

REFERENCES

T. Sakanoi, Y. Kasaba, M. Kagitani, H. Nakagawa, J. Kuhn, and S. Okana, "Development of infrared echelle spectrograph and mid-infrared heterodyne spectrometer on a small telescope at Haleakala, Hawaii for planetary observation," Proc. SPIE 9147, 91478D (2014).

- J. Qiu, X. Qi, X. Li, Z. Ma, Jirigalantu, Y. Tang, X. Mi, X. Zheng, and Bayanheshig, "Development of a spatial heterodyne Raman spectrometer with echelle-mirror structure," Opt. Express 26, 11994–12006 (2018).
- B. Zhang, Z. Wang, S. Brodbeck, C. Schneider, M. Kamp, S. Höfling, and H. Geng, "Zero-dimensional polariton laser in a subwavelengh grating-based vertical microcavity," Light Sci. Appl. 3, e135 (2014).
- F. Cheng, J. Zhang, D. Wang, Z. Gu, N. Zhuo, S. Zhai, L. Wang, J. Liu, S. Liu, and Z. Wang, "Demonstration of high-power and stable singmode in a quantum cascade laser using buried sampled grating," Nanoscale Res. Lett. 14. 123 (2019).
- T. Lei, M. Zhang, Y. Li, P. Jia, G. Ning Liu, X. Xu, Z. Li, C. Min, J. Lin, C. Yu, H. Niu, and X. Yuan, "Massive individual orbital angular momentum channels for multiplexing enabled by Dammann gratings," Light Sci. Appl. 4, e257 (2015).
- H. Xu and Y. Shi, "Subwavelength-grating-assited silicon polarization rotator covering all optical communication bands," Opt. Express 27, 5588–5597 (2019).
- A. Cotel, M. Castaing, P. Pichon, and C. Le Blanc, "P hased-array grating compression for high-energy chirped pulse amplification lasers," Opt. Express 15, 2742–2752 (2007).
- J. Qiao, A. W. Schmid, L. J. Waxer, T. Nguyen, J. Bunkenburg, C. Kingsley, A. Kozlov, and D. Weinerl, "In situ detection and analysis of laser-induced damage on a 1.5-m multilayer-dielectric grating compressor for high-energy, petawatt-class laser systems," Opt. Express 18, 10423–10431 (2010).
- S. Zhang, X. Mi, Q. Zhang, Jirigalantu, S. Feng, H. Yu, and X. Qi, "Groove shape characteristics of echelle gratings with high diffraction efficiency," Opt. Commun. 387, 401–404 (2017).
- D. Nevejans, E. Neefs, E. Van Ransbeeck, S. Berkenbosch, R. Clairquin, L. De Vos, W. Moelans, S. Glorieux, A. Baeke, O. Korablev, I. Vinogradov, Y. Kalinnikov, B. Bach, J.-P. Dubois, and E. Villard, "Compact high-resolution spaceborne echelle grating spectrometer

- with acousto-optical tunable filter based order sorting for the infrared domain from 2.2 to 4.3 μ m," Appl. Opt. **45**, 5191–5206 (2006).
- G. R. Harrison and S. W. Thompson, "Large diffraction gratings ruled on a commercial measuring machine controlled interferometrically," J. Opt. Soc. Am. 60, 591–595 (1970).
- T. Kita and T. Harada, "Ruling engine using a piezoelectric device for large and high-groove density gratings," Appl. Opt. 31, 1399–1406 (1992).
- X. Mi, H. Yu, H. Yu, S. Zhang, X. Li, X. Yao, X. Qi, Bayinheshig, and Q. Wang, "Correcting groove error in gratings ruled on a 500-mm ruling engine using interferometric control," Appl. Opt. 56, 5857–5864 (2017).
- X. Mi, S. Zhang, X. Qi, H. Yu, J. Zhou, and S. Jiang, "Effect of thickness non-uniformity of large-area grating metal film on grating diffraction wavefront," Opt. Laser Technol. 119, 105675 (2019).
- X. Mi, S. Zhang, H. Yu, H. Yu, M. Cong, and X. Qi, "Using a unique mirror to minimize the effect of ruling engine cosine error on grating performance," Appl. Opt. 57, 10146–10151 (2018).
- X. Mi, S. Zhang, X. Qi, H. Yu, H. Yu, Y. Lin, X. Yao, S. Jiang, and J. Zhou, "Effect of the changes in refractive index of air on grating diffraction wavefront," Opt. Commun. 457, 124716 (2020).
- G. R. Harrison, S. W. Thompson, H. Kazukonis, and J. R. Connell, "750-mm ruling engine producing large gratings and echelles," J. Opt. Soc. Am. 62, 751–756 (1972).
- X. Li, H. Yu, X. Qi, S. Feng, J. Chui, S. Zhang, Jirigalantu, and Y. Tang, "300 mm ruling engine producing gratings and echelles under interferometric control in China," Appl. Opt. 54, 1819–1826 (2015).
- X. Mi, S. Zhang, X. Qi, H. Yu, H. Yu, and Y. Tang, "Ruling engine using adjustable diamond and interferometric control for high-quality gratings and large echelles," Opt. Express 27, 19448–19462 (2019).